Author's Accepted Manuscript

An evaluation of the hexagonal close-packed to face-centered cubic phase transformation in a Ti-6Al-4V alloy during high-pressure torsion

Hamed Shahmir, Terence G. Langdon

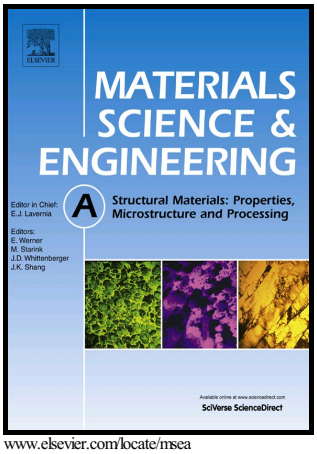

www.elsevier.com/locate/msea

PII: S0921-5093(17)31004-3
DOI: http://dx.doi.org/10.1016/j.msea.2017.07.099
Reference: MSA35347

To appear in: *Materials Science & Engineering A*

Received date: 17 July 2017
Revised date: 30 July 2017
Accepted date: 31 July 2017

Cite this article as: Hamed Shahmir and Terence G. Langdon, An evaluation o the hexagonal close-packed to face-centered cubic phase transformation in a Ti 6Al-4V alloy during high-pressure torsion, *Materials Science & Engineering A* http://dx.doi.org/10.1016/j.msea.2017.07.099

This is a PDF file of an unedited manuscript that has been accepted fo publication. As a service to our customers we are providing this early version o the manuscript. The manuscript will undergo copyediting, typesetting, an review of the resulting galley proof before it is published in its final citable form Please note that during the production process errors may be discovered whic could affect the content, and all legal disclaimers that apply to the journal pertain

ACCEPTED MANUSCRIPT

An evaluation of the hexagonal close-packed to face-centered cubic phase transformation in a Ti-6Al-4V alloy during high-pressure torsion

Hamed Shahmir, Terence G. Langdon*

Materials Research Group, Faculty of Engineering and the Environment, University of Southampton, Southampton SO17 1BJ, UK

*Corresponding author. Tel.: +44-2380594438. langdon@soton.ac.uk

Abstract

A Ti-6Al-4V alloy was used to examine the effect of martensitic (α') or lamellar (α+β) microstructures on grain refinement and the *hcp* to *fcc* phase transformation during HPT processing. There was significant grain refinement with grain sizes of ~30 and ~40 nm in the α' and α+β microstructures, respectively, and with the occurrence of an allotropic *hcp* to *fcc* phase transformation in the α' sample after HPT. A high volume fraction of boundaries, together with a substructure containing initial defects of the martensitic sample, promotes the formation of the *fcc* phase during the HPT processing.

Keywords: high-pressure torsion; nanostructured materials; phase transformation; severe plastic deformation; Ti-6Al-4V alloy.

Accepted manuscript

1. Introduction

It is well known that titanium and its alloys display different phases depending on the pressure and temperature. The Ti-6Al-4V alloy is an α (*hcp*) +β (*bcc*) alloy at room temperature but a fully or partly martensitic type of α' (*hcp*) and α" (orthorhombic) forms using a high cooling rate in the α+β region or above the β-transus temperature (990 ± 20 °C) [1]. In addition, an *fcc* phase was reported in an investment cast Ti-6Al-4V alloy during different heat treatment processes [2] and very recently in a surface layer after high energy shot peening [3]. Basically, the formation of the *fcc* phase is not anticipated from the

ACCEPTED MANUSCRIPT

equilibrium phase diagram of Ti [4], but there are experiments showing an *fcc* structure in very thin epitaxial films [5,6] and in high-energy milled powders [7,8]. Very recently, an *hcp* to *fcc* phase transformation was reported in a bulk commercial purity α-Ti during cryogenic channel die compression [9] and cold rolling [10].

Processing through the application of severe plastic deformation (SPD) leads to significant grain refinement but may also affect the phase stability of various metals and alloys. High-pressure torsion (HPT) is a well-established SPD procedure [11-13] and in pure Ti it was established that there may be an α (*hcp*) to ω (*hcp*) phase transformation during HPT processing [14-17]. Similarly, HPT-induced β to ω [18] and α" to ω [19] phase transformations were reported in a Ti-Nb alloy. Nevertheless, no phase transformation was detected and there was only β-phase dissolution during HPT processing of a Ti-6Al-4V alloy [20-24]. In the present work, a Ti-6Al-4V alloy was subjected to two different heat treatments in order to produce initial microstructures that were either almost fully martensitic α' or fully lamellar α+β. Research was then conducted to provide information on the significance of the initial microstructural condition prior to HPT processing on the subsequent microstructure, the occurrence of any phase transformations and the levels of grain refinement achieved within the alloy.

2. Experimental material and procedures

The experiments were conducted using a Ti-6Al-4V alloy where the composition is given in wt%. Prior to processing by HPT, the material was divided into two separate batches and these two batches were prepared using different heat treatments. The first batch was subjected to a solution annealing at 1000 °C for 30 min followed by water quenching to obtain a martensitic α' microstructure. The second batch was solution annealed at 950 °C for 45 min, air cooled to room temperature and then given a stress relief anneal at 600 °C for 3 h under an Ar-controlled atmosphere followed by furnace cooling to obtain a lamellar α+β

Accepted manuscript

ACCEPTED MANUSCRIPT

microstructure. Following the initial heat treatments, disks with thicknesses of ~0.8 mm and diameters of 10 mm were processed by HPT at room temperature under an applied pressure of P = 6.0 GPa using a rotation speed of 1 rpm and rotations through totals of 1, 5 and 10 revolutions under quasi-constrained conditions [25].

After HPT processing, each disk was polished to a mirror-like quality and then hardness measurements were taken using a Vickers microhardness tester with a load of 500 gf and dwell times of 10 s. The average microhardness values, Hv, were measured along randomly selected diameters on each disk with the measurements taken at intervals of ~0.5 mm and at every point the local value of Hv was obtained from an average of four separate hardness measurements. The phase constituents were determined using X-ray diffraction (XRD) (Rigaku SmartLab) employing Cu Kα radiation (wavelength λ = 0.154 nm) at 45 kV with a tube current of 200 mA. The XRD measurements were performed over a 2θ range from 30° to 90° using a scanning step of 0.01° and a scanning speed of 2° min^{-1}. The analysis for XRD was conducted using sample areas with diameters of 3 mm located near the edges of the disks. Foils for transmission electron microscopy (TEM) were prepared using a focused ion beam (FIB) method at 3 mm from the disk centres in the normal section of the disks so that the normal of the image lies in the shear direction.

Accepted manuscript

3. Experimental results

Figure 1(a) shows the microstructure after the first heat treatment including the coarse prior-β grains, indicated by dashed lines, with an average size of ~500 μm and fully transformed to martensite. The microstructure in Fig. 1(a) shows martensitic laths having different orientations distributed throughout the microstructure with an average lath thickness of ~0.8 μm. Figure 1(b) shows the microstructure after the second heat treatment including a lamellar α+β structure with different orientations and with a retained β-phase lying between

ACCEPTED MANUSCRIPT

the α platelets. The resulting microstructure contained an average prior-β grain size of ~500 μm, packets of parallel-oriented α+β lamellae of ~200 μm and an average α lamellar lath width of ~1.5 μm. Close inspection of Fig. 1(b) shows a grain boundary allotriomorph α-phase marked by an arrow which begins to form as soon as the temperature drops below the β transus temperature.

The variation of hardness with equivalent strain is shown in Fig. 2 for the two groups of samples processed through up to 10 turns. This plot confirms that the datum points reach saturation hardnesses of ~390 and ~350 for the α' and α+β samples, respectively, after similar equivalent strains of ~50. The results in Fig. 2 demonstrate that the overall microhardess of the martensitic sample is higher than the lamellar sample after HPT processing but nevertheless it is apparent that the general hardenability of the lamellar sample is higher than for the martensitic sample.

Figure 3 shows the X-ray diffraction patterns at the edges of the disks for (a) the α' and (b) the α+β samples before (N = 0) and after HPT processing through 1 to 10 turns. In Fig. 3(a) for N = 0, the first heat treatment produces a martensitic microstructure and there is a main peak of $(101)_{\alpha/\alpha'}$. The XRD pattern at N = 0 after the second heat treatment shown in Fig. 3(b) represents α-phase peaks and a peak corresponding to the $(110)_{\beta}$ plane at $2\theta \approx 39.6°$. The volume fraction of the β-phase for this condition was only ~6% as calculated using standard procedures [26]. Close inspection of Fig. 3(a) shows the appearance of new peaks in the α' sample after HPT through 5 and 10 turns at 2θ = 44.5° and 64.4° marked with open triangles where this corresponds to the typical (200) and (220) planes of the *fcc* structure. According to these results, the lattice parameter of this *fcc* phase is $a \approx 4.1$ Å. The patterns in Fig. 3(a) and a plot presented in Fig. 4 also illustrate the effect of the numbers of rotations on the α to *fcc*-phase transformation since the intensities of the *fcc*-phase peaks increase with increasing numbers of revolutions up to ~40% after 10 turns. Nevertheless, for the α+β

Accepted manuscript

ACCEPTED MANUSCRIPT

sample in Fig. 3(b) no *fcc* or β phases are present in the X-ray diffraction patterns. Therefore, these results confirm a dissolution of the β-phase during HPT processing which is consistent with an earlier report [20].

Peak broadenings were examined for determinations of the grain size and dislocation density in the HPT-processed sample using the classic Williamson-Hall method as [27,28]:

$$\frac{2(\Delta\theta)cos\theta}{\lambda} = \frac{0.9}{d} + \frac{2\varepsilon\, sin\theta}{\lambda} \quad (1)$$

where ε represents the broadening resulting from strain and d is the average grain size, $\Delta\theta$, λ and θ are the structural full width at half maximum (FWHM), X-ray wavelength (0.154 nm for Cu) and the diffraction angle, respectively. The derivation of the structural peak breadths were performed according to the Stokes method as given by $\Delta\theta^2 = \Delta\theta_{exp}^2 - \Delta\theta_{ins}^2$ for a Gaussian function, where $\Delta\theta_{exp}$and $\Delta\theta_{ins}$ are the experimental (HPT sample) and instrumental (as heat-treated sample) FWHM, respectively. After the removal of the instrumental broadening, the structural FWHM, $\Delta\theta$, of the diffraction peak profiles were considered for the above equation. Thus, a plot of $2\Delta\theta cos\theta/\lambda$ versus $2sin\theta/\lambda$ should give a straight line of gradient ε and an intercept of $1/d$. Figure 5 displays this plot for the α' and α+β alloy after HPT through 10 turns. An increase in the crystalline defects density is the most prominent phenomenon taking place during HPT.

In order to estimate the dislocation density for each condition, the following simple equation may be used [28]:

$$\rho = \frac{2\sqrt{3}\varepsilon}{bd} \quad (2)$$

where ρ and b are the dislocation density and the Burgers vector, respectively. Considering the Burgers vector, b, of the <*a*> dislocation (b = 0.295 nm) as the dominant dislocation type during deformation [29], the grain size, strain and dislocation density of α' after HPT were estimated as ~25 nm, ~0.023 and ~11 × 10^{15} m^{-2}, respectively. In addition, the corresponding

ACCEPTED MANUSCRIPT

values for the α+β sample after HPT were ~30 nm, ~0.019 and ~7.2 × 10^{15} m^{-2}, respectively. Therefore, the martensitic sample has a smaller grain size and a higher dislocation density after HPT which is consistent with its higher hardness.

The microstructures and corresponding SAED patterns of the α' and α+β samples are shown in Fig. 6 (a,c,e) and Fig. 6 (b,d,f) after HPT through 10 turns at a region of ~3 mm from the disk centre. The microstructure of the α' sample consists of faint nanolamellae with thicknesses of ~20 to 50 nm as marked with dashed lines in Fig. 6(a) and a highly dislocated substructure with some equiaxed nanograins having an average size of ~30 nm. It appears that the nanolamellae contain non-uniform contrasts because of the presence of areas with high and low densities of lattice defects. The microstructures of the α+β sample (Fig. 6b) consist of arrays of ultrafine equiaxed grains having average sizes of ~40 nm without nano-lamellar features. Frequently extended areas containing numerous small overlapping grains are visible in Fig. 6(c) and (d) with Moiré fringes of periodicity [30]. In Fig. 6(c) and (d) there are some very small grains shown by arrows which are essentially dislocation-free and some grains shown by circles containing nanotwins. Nevertheless, the observations indicate that these nonotwins are not common in the microstructure of the α+β sample. The arrangements of the diffraction spots in semi-continuous circles in the SAED patterns, represented in Fig. 6(e) and (f), confirm that the microstructures contain boundaries having high angles of misorientation. An examination of the SAED pattern in Fig. 6(e) shows the existence of *fcc* and *hcp* phases in the microstructure of the α' sample after HPT and this is consistent with the XRD result in Fig. 6(a). It is important to note that the grain sizes measured from the images are consistent with the calculated values.

4. Discussion

The present results show that significant grain refinement is achieved through HPT with average grain sizes of ~30 and ~40 nm in the α' and α+β samples, respectively. It is

Accepted manuscript

ACCEPTED MANUSCRIPT

important to note that the smallest grain size reported earlier for a Ti-6Al-4V alloy was $d \approx 75 \pm 15$ nm for a sample containing 25% α-phase and 75% lamellar (α+β) and processed by HPT for up to 20 turns [24]. It is known that grain refining by HPT becomes more effective as the volume fraction of the lamellar increases since the boundaries may act as nucleation sites for high-speed grain fragmentation together with subgrain formation during the initial stages of deformation [31].

The behavior of the α′ microstructure is due to the high level of residual stress and the large volume of initial defects which provide nucleation sites for dislocations, stacking faults, interfaces of martensite variants and twins [32], together with the high-speed grain fragmentation and subgrain formation in the α′ initial microstructure in the early stages of HPT. The lack of strain hardening in the α′ sample is due to the small dislocation cell and grain sizes together with the high defect density in the initial state by comparison with the α+β sample. In the as-processed material, it is reasonable to anticipate that the defect storage is probably close to the saturation limit for the α′ sample.

Despite the differences in the initial microstructures, it should be noted that the crystal structures for both of these samples for these two heat treatments are *hcp*. The results show clearly that the volume fraction of the β (*bcc*) phase in the α+β sample is only 6% and therefore it is unlikely that this phase controls the hardening. It is well known that twinning plays an important role in the deformation of coarse-grained *hcp* Ti due to an insufficient number of slip systems and it is concluded that twining played a major role in grain refinement at least in the early stages of deformation [33-35]. This will lead to local stress concentrations and the so-called dynamic Hall-Petch effect [36]. It was established earlier that the twins break up into subcells after large amounts of deformation and also the twinning propensity decreases with decreasing grain size in Ti during SPD [34]. Therefore, a new mechanism is needed to accommodate the deformation such as dislocation slip [37] or phase

Accepted manuscript

ACCEPTED MANUSCRIPT

transformations. The existence of high dislocation densities in the TEM images in Fig. 6(a) suggests that dislocation slip is the primary deformation mechanism in the later stage of SPD. In addition, the results indicate that an *hcp* to *fcc* phase transformation plays an important role in accommodating the constrained deformation in the high defect martensitic sample.

It was reported that the α (*hcp*) to ω (*hcp*) and α (*hcp*) to *fcc* phase transformation can accommodate macro-strains comparable to compression twins in Ti [10] but it is important to note that an α (*hcp*) to ω (*hcp*) phase transformation was not observed in this research. Nevertheless, this phase was observed in commercially pure Ti as an additional plastic deformation mode comparable to twinning [16,17] after the same experimental procedure. An important parameter governing the α to ω transformation is the role of impurities in Ti, in particular the oxygen content [38] and it seems that this parameter is very important in suppressing the α to ω transformation in the Ti-6Al-4V alloy which contains 6% Al and 4% V and also 650 ppm oxygen where this is higher than CP-Ti with ~250 ppm oxygen [17]. Nevertheless, there is clear evidence for the *hcp* to *fcc* phase transformation in the α′ sample during HPT processing through more than 1 revolution and this transformation in Ti is therefore attributed to a combination of structural instability due to grain refinement, an increasing lattice expansion, plastic straining and the density and influence of crystal defects introduced during processing [8]. Stacking faults may also play an important role in this phase transformation in the α′ sample and the importance of these faults was considered earlier in the *hcp* to *fcc* transformation in a Ti-20Zr-6.5Al-4V alloy [39].

The *hcp* to *fcc* phase transformation in the α′ sample may be accomplished during HPT through the gliding of Shockley partial dislocations on every two *hcp* planes. Considering a combination of Shockley partial dislocations, a macroscopic strain will accompany the phase transformation when all Shockley partials have the same Burgers vector or alternatively the transformation will not generate a macroscopic strain in the so-called

Accepted manuscript

ACCEPTED MANUSCRIPT

zero-strain transformation [40,41] when the net Burgers vector of all Shockley partials is equal to zero. The *fcc* and *hcp* phases take orientation relations given by $\{10\text{-}10\}_{hcp}||\{110\}_{fcc}$ and $\langle 0001\rangle_{hcp}||\langle 001\rangle_{fcc}$ whch are different from the well-known *fcc-hcp* orientation relation. In practice, the nucleation of the *fcc* phase is accomplished via a pure-shuffle mechanism involving Shockley partial dislocations of $a/6\ \langle 11\text{-}20\rangle$-type gliding on [10-10] prism planes [9].

The results of this investigation show that grains having sizes smaller than ~40 nm are dislocation-free. Therefore, the emission of partial dislocations may dominate in these grains by subsequent deformation. Then partial dislocation emission from the grain boundaries will become a major mechanism for the *hcp* to *fcc* phase transformation at very small grain sizes and this explains the formation of *fcc* nanograins. The microstructure of the α′ (*hcp*) sample contains a high volume fraction of boundaries and a substructure containing predominately dislocations and stacking faults with a few platelets containing twins. This microstructure leads to significant grain refinement and these defects therefore promote refinement and the formation of the *fcc* phase during HPT processing.

5. Summary and conclusions

1. A Ti-6Al-4V alloy was given two different heat treatments to produce either α′ or lamellar α+β initial microstructures and then processed by HPT under a pressure of 6.0 GPa for up to 10 turns at room temperature. Microhardness measurement showed saturation hardnesses of ~390 and ~340 after an equivalent strain of ~50 for the α′ and α+β samples, respectively. The results demonstrate that the microhardness of the α′ sample is higher and the hardenability is lower by comparison with the α+β sample after HPT processing.

2. Microstructural examination showed exceptional grain refinement in the α′ sample with a grain size of ~30 nm and a high dislocation density of $\sim 11 \times 10^{15}$ m^{-2} at the saturation

Accepted manuscript

ACCEPTED MANUSCRIPT

level of microhardness after HPT processing. In the α+β sample, the grain size was reduced to ~40 nm with a dislocation density of ~7.2×10^{15} m^{-2}.

3. An *hcp* to *fcc* phase transformation occurred during HPT processing of the α' sample but not in the early stages of straining. This phase transformation was activated to accommodate the strain produced during HPT and the martensitic microstructure consisted of very thin laths of ~0.8 μm and a high volume fraction of boundaries. The substructure contained predominately dislocations and stacking faults with a few platelets containing twins. The propensity for the formation of the *fcc* phase was significantly higher in the α' sample.

Acknowledgement

This work was supported by the European Research Council under Grant Agreement No. 267464-SPDMETALS.

References

1. B.K. Damkroger, G.R. Edwards, Continuous cooling transformation kinetics in alpha-beta titanium alloys, In: *Simulation and theory of evolving microstructure*, M.P. Anderson and A.D. Rollett, eds, The Minerals, Metals and Materials Society, Warrendale, PA, 1990, 129-152.
2. M.T. Jovanović, S. Tadić, S. Zec, Z. Mišković, I. Bobić, The effect of annealing temperatures and cooling rates on microstructure and mechanical properties of investment cast Ti-6Al-4V alloy, Mater. Design 27 (2006) 192-199.
3. Y.G. Liu, M.Q. Li, H.J. Liu, Deformation induced face-centered cubic titanium and its twinning behaviour in Ti-6Al-4V, Scr. Mater 119 (2016) 5-8.

Accepted manuscript

ACCEPTED MANUSCRIPT

4. D.A. Young, Phase diagrams of the elements. Berkeley, CA: University of California Press, 1991.
5. A.A. Saleh, V. Shutthanandan, R.J. Smith, Observation of ultrathin metastable fcc Ti films on Al (110) surfaces, Phys. Rev. B 49 (1994) 4908-4914.
6. A.F. Jankowski, M.A. Wall, Formation of face-centered cubic titanium on a Ni single crystal and in Ni/Ti multilayers, J. Mater. Res. 9 (1994) 31-38.
7. Y. Sugawara, N. Shibata, S. Hara, Y. Ikuhara, Interface structure of face-centered-cubic-Ti thin film grown on 6H-SiC substrate, J. Mater. Res. 15 (2000) 2121-2124.
8. P. Chatterjee, S.P. Sen Gupta, An X-ray diffraction study of strain localization and anisotropic dislocation contrast in nanocrystalline titanium, Philos. Mag. A 81 (2001) 49-60.
9. D.H. Hong, T.W. Lee, S.H. Lim, W.Y. Kim, S.K. Hwang, Stress-induced hexagonal close-packed to face-centered cubic phase transformation in commercial-purity titanium under cryogenic plane-strain compression, Scr. Mater. 69 (2013) 405-408.
10. H.C. Wu, A. Kumar, J. Wang, X.F. Bi, C.N. Tomé, Z. Zhang, S.X. Mao, Rolling-induced face centered cubic titanium in hexagonal close packed titanium at room temperature, Sci. Report. 6 (2016) 24370 (1-8).
11. R.Z. Valiev, R.K. Islamgaliev, I.V. Alexandrov, Bulk nanostructured materials from severe plastic deformation, Prog. Mater. Sci. 45 (2000) 103-189.
12. A.P. Zhilyaev, T.G. Langdon, Using high-pressure torsion for metal processing: Fundamentals and applications, Prog. Mater. Sci. 53 (2008) 893-979.
13. T.G. Langdon, Twenty-five years of ultrafine-grained materials: Achieving exceptional properties through grain refinement, Acta Mater. 61 (2013) 7035-7059.
14. Y. Ivanisenko, A. Kilmametov, H. Rösner, R.Z. Valiev, Evidence of α→ω phase transition in titanium after high pressure torsion, Int J Mat Res 99 (2008) 36-41.

Accepted manuscript

ACCEPTED MANUSCRIPT

15. Y. Todaka, J. Sasaki, T. Moto, M. Umemoto, Bulk submicrocrystalline ω-Ti produced by high-pressure torsion straining, Scr. Mater. 59 (2008) 615-618.
16. K. Edalati, E. Matsubara, Z. Horita, Processing pure Ti by high-pressure torsion in wide ranges of pressures and strain, Metall. Mater. Trans. A 40 (2009) 2079-2089.
17. H. Shahmir, T.G. Langdon, Characteristics of the allotropic phase transformation in titanium processed by high-pressure torsion using different rotation speeds, Mater. Sci. Eng. A667 (2016) 293-299.
18. Y.B. Wang, Y.H. Zhao, Q. Lian, X.Z. Liao, R.Z. Valiev, S.P. Ringer, Y.T. Zhu, E.J. Lavernia, Grain size and reversible beta to omega phase transformation in a Ti alloy, Scr. Mater. 63 (2010) 613-616.
19. A. Panigrahi, M. Bönisch, T. Waitz, E. Schafler, M. Calin, J. Eckert, W. Skrotzki, M. Zehetbauer, Phase transformations and mechanical properties of biocompatible Ti-16.1Nb processed by severe plastic deformation, J. Alloys Compds 628 (2015) 434-441.
20. A.V. Sergueeva, V.V. Stolyarov, R.Z. Valiev, A.K. Mukherjee, Enhanced superplasticity in a Ti-6Al-4V alloy processed by severe plastic deformation, Scr. Mater. 43 (2000) 819-824.
21. R.S. Mishra, V.V. Stolyarov, C. Echer, R.Z. Valiev, A.K. Mukherjee, Mechanical behavior and superplasticity of a severe plastic deformation processed nanocrystalline Ti-6Al-4V alloy, Mater. Sci. Eng. A 298 (2001) 44-50.
22. A.V. Sergueeva, V.V. Stolyarov, R.Z. Valiev, A.K. Mukherjee, Superplastic behaviour of ultrafine-grained Ti–6A1–4V alloys, Mater. Sci. Eng. A 323 (2002) 318-325.
23. Y.C. Wang, T.G. Langdon, Influence of phase volume fractions on the processing of a Ti-6Al-4V alloy by high-pressure torsion, Mater. Sci. Eng. A 559 (2013) 861-867.

Accepted manuscript

ACCEPTED MANUSCRIPT

24. J. Fu, H. Ding, Y. Huang, W. Zhang, T.G. Langdon, , Influence of phase volume fraction on the grain refining of a Ti-6Al-4V alloy by high-pressure torsion, J. Mater. Res. Technol. 4 (2015) 2-7.

25. R.B. Figueiredo, P.R. Cetlin, T.G. Langdon, Using finite element modeling to examine the flow processes in quasi-constrained high-pressure torsion, Mater. Sci. Eng. A 528 (2011) 8198-8204.

26. B.D. Cullity, S.R. Stock, Elements of X-ray Diffraction. 3rd Ed, Prentice Hall, Englewood Cliffs, NJ, U.S.A. 2001.

27. G.K. Williamson, W.H. Hall, X-ray line broadening from filed aluminium and wolfram, Acta Metall. 1 (1953) 22-31.

28. G.K. Williamson, R.E. Smallman, Dislocation densities in some annealed and cold-worked metals from measurements on the X-ray debye-scherrer spectrum, Phil. Mag. 1 (1956) 34-45.

29. Y.T. Zhu, J.Y. Huang, J. Gubicza, T. Ungár, Y.M. Wang, E. Ma, R.Z. Valiev, Nanostructures in Ti processed by severe plastic deformation, J. Mater. Res. 18(8) (2003) 1908-1917.

30. C. Rentenberger, T. Waitz, H.P. Karnthaler, HRTEM analysis of nanostructured alloys processed by severe plastic deformation, Scr. Mater. 51 (2004) 789-794.

31. P. Castany, F. Pettinari-Sturmel, J. Douin, A. Coujou, In situ transmission electron microscopy deformation of the titanium alloy Ti-6Al-4V: Interface behaviour, Mater. Sci. Eng. A 483-484 (2008) 719-722.

32. F.J. Gil, J.M. Manero, J.A. Planell, Decomposition of α′ martensite plates of Ti-6Al-4V alloy at different annealing temperatures and heat treatment times. In: *Titanium 1995, Science and Technology*, P.A. Blankensop, W.J. Evans, H.M. Flower (eds.), The Institute of Materials, London, UK, (1996) 2454-2461.

Accepted manuscript

ACCEPTED MANUSCRIPT

33. D.H. Shin, I. Kim, J. Kim, Y.T. Zhu, Shear strain accommodation during severe plastic deformation of titanium using equal channel angular pressing, Mater. Sci, Eng. A 334 (2002) 239-245.

34. D.H. Shin, I. Kim, J. Kim, Y.S. Kim, S.L. Semiatin, Microstructure development during equal-channel angular pressing of titanium, Acta Mater. 51 (2003) 983-996.

35. S.V. Zherebtsov, G.S. Dyakonov, A.A. Salem, S.P. Malysheva, G.A. Salishchev, S.L. Semiatin, Evolution of grain and subgrain structure during cold rolling of commercial-purity titanium, Mater. Sci. Eng. A 528 (2011) 3474-3479.

36. A.A. Salem, S.R. Kalidindi, R.D. Doherty, Strain hardening of titanium: role of deformation twinning, Acta Mater. 51 (2003) 4225-4237.

37. M.H. Yoo, twinning, and fracture in hexagonal close-packed metals, Metall. Trans. 12A (1981) 409-418.

38. Y. Lu, H. Yang, G. Tan, S. Miyazaki, B. Jiang, Y. Liu, Stress-induced FCC→ HCP martensitic transformation in CoNi, J. Alloys Compds 368 (2004) 157-163.

39. R. Jing, C.Y. Liu, M.Z. Ma, R.P. Liu, Microstructural evolution and formation mechanism of FCC titanium during heat treatment processing. J. Alloys Compds 552 (2013) 202-207.

40. T. Waitz, H.P. Karnthaler, Transformation strains in martensitic phase transitions of Co alloys, Phase Transit. 67 (1999) 695-705.

41. L. Liu, J. Wang, S.K. Gong, S.X. Mao, High resolution transmission electron microscope observation of zero-strain deformation twinning mechanisms in Ag. Phys. Rev. Lett. 106 (2011) 175504.

Accepted manuscript

ACCEPTED MANUSCRIPT

Fig. 1 Optical micrographs of microstructures of the Ti-6Al-4V alloy after (a) annealing at 1000°C for 30 min followed by water quenching (α' alloy): dotted lines represent prior β grain boundaries; (b) annealing at 950°C for 45 min followed by air quenching and then annealing at 600°C for 3 h followed by furnace quenching (α+β alloy); a grain boundary allotriomorph α-phase is shown by the arrow.

Fig. 2 Values of the Vickers microhardness plotted against equivalent strain after processing by HPT through various numbers of turns.

Fig. 3 X-ray patterns of (a) the α' and (b) the α+β alloys near the edges of the disks before (N = 0) and after HPT processing through 1 to 10 turns.

Fig. 4 Volume fraction of *fcc* phase plotted against the number of rotations for the α' samples, near the edges of the disks before (N = 0) and after HPT processing through 1 to 10 turns.

Fig. 5 Classical Williamson-Hall plots for α' and α+β samples processed by HPT through 10 turns.

Fig. 6 TEM images and corresponding SAED patterns of (a,c,e) α' and (b,d,f) α+β samples after 10 turns of HPT; nanograins and nanolamellar structure of 20 to 50 nm thickness marked with dashed line where dislocation density within some nanolamellars is higher than in their neighbours in α' sample; banded contrast represents moiré patterns and appears as a result of overlapping of nano-sized grains, and some dislocation-free grains and grains containing nanotwins are marked by arrows and circles, respectively.

Accepted manuscript

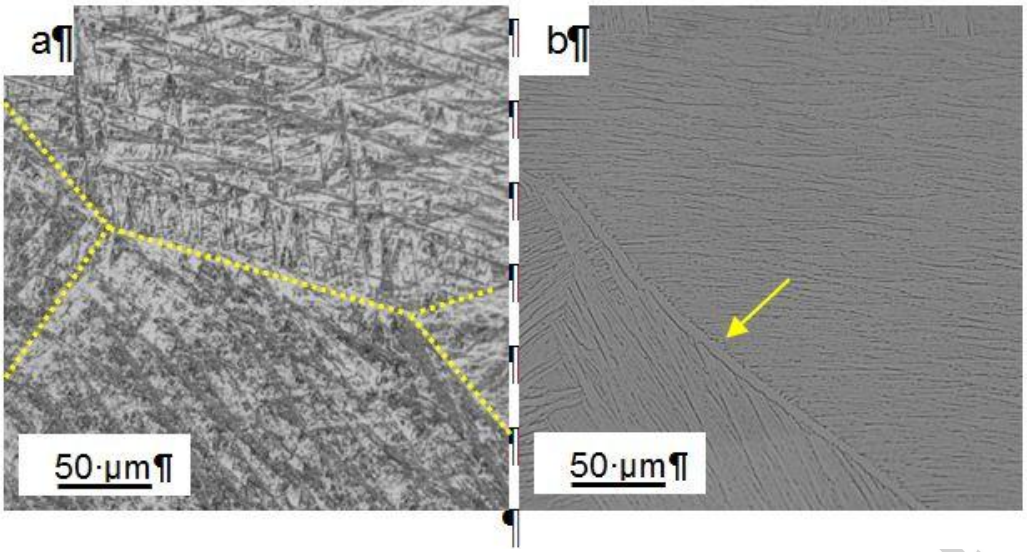
a¶
b¶
50·µm¶
50·µm¶

Fig. 1

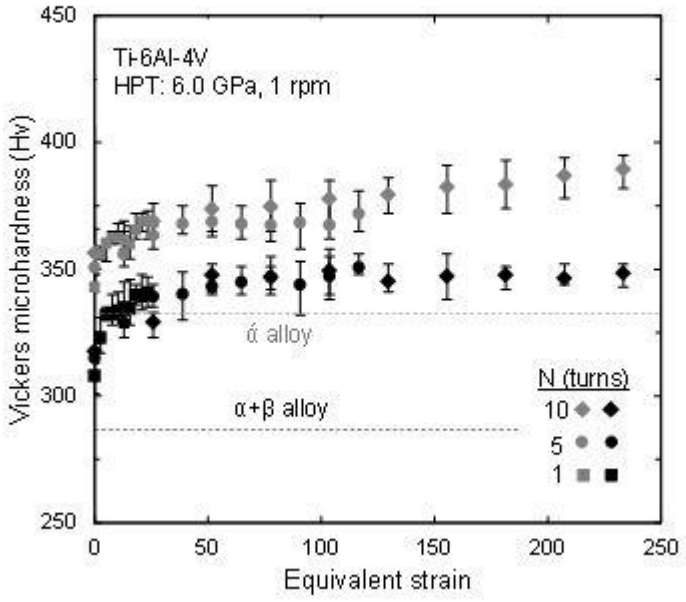
Ti-6Al-4V
HPT: 6.0 GPa, 1 rpm
Vickers microhardness (Hv)
Equivalent strain
α alloy
α+β alloy
N (turns)
10
5
1
450
400
350
300
250
0
50
100
150
200
250

Fig. 2

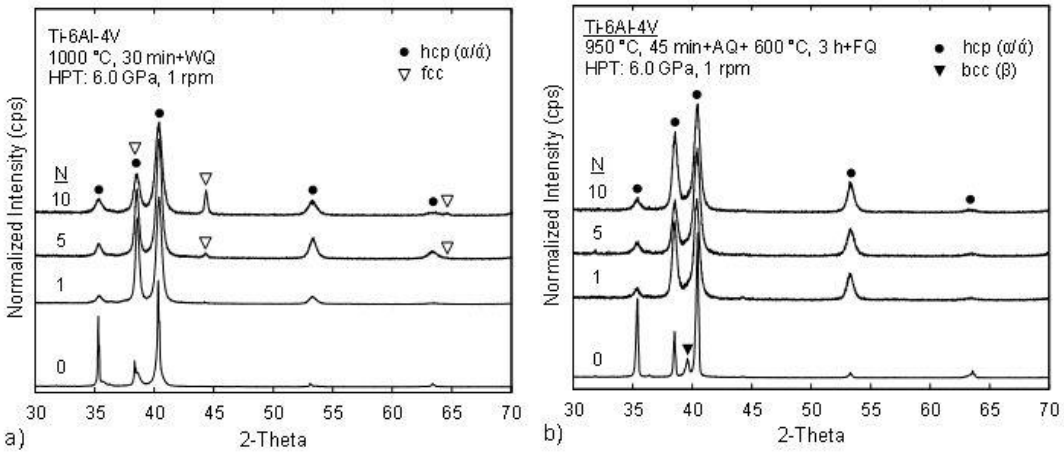
Ti-6Al-4V
1000 °C, 30 min+WQ
HPT: 6.0 GPa, 1 rpm
hcp (α/ά)
fcc
N
10
5
1
0
Normalized Intensity (cps)
2-Theta
a)
Ti-6Al-4V
950 °C, 45 min+AQ+ 600 °C, 3 h+FQ
HPT: 6.0 GPa, 1 rpm
hcp (α/ά)
bcc (β)
b)

Fig. 3

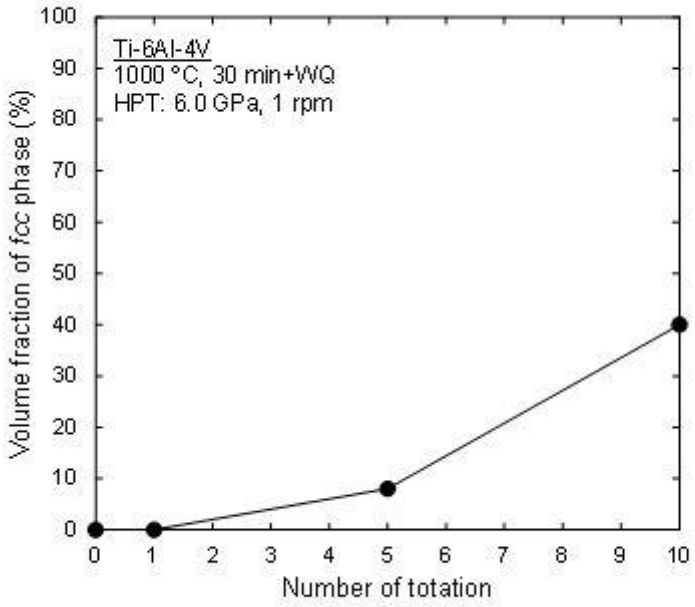
Ti-6Al-4V
1000 °C, 30 min+WQ
HPT: 6.0 GPa, 1 rpm
Volume fraction of fcc phase (%)
Number of totation

Fig. 4

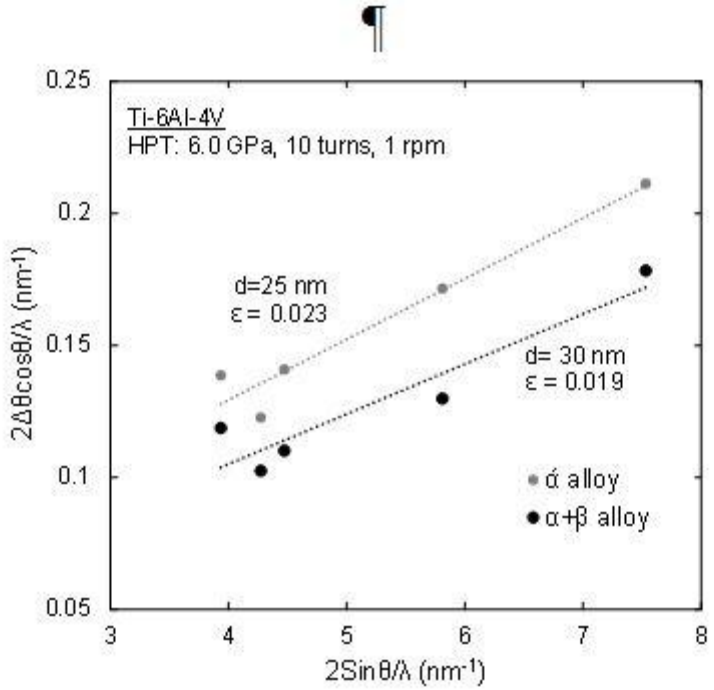

Fig. 5

Accepted manuscript

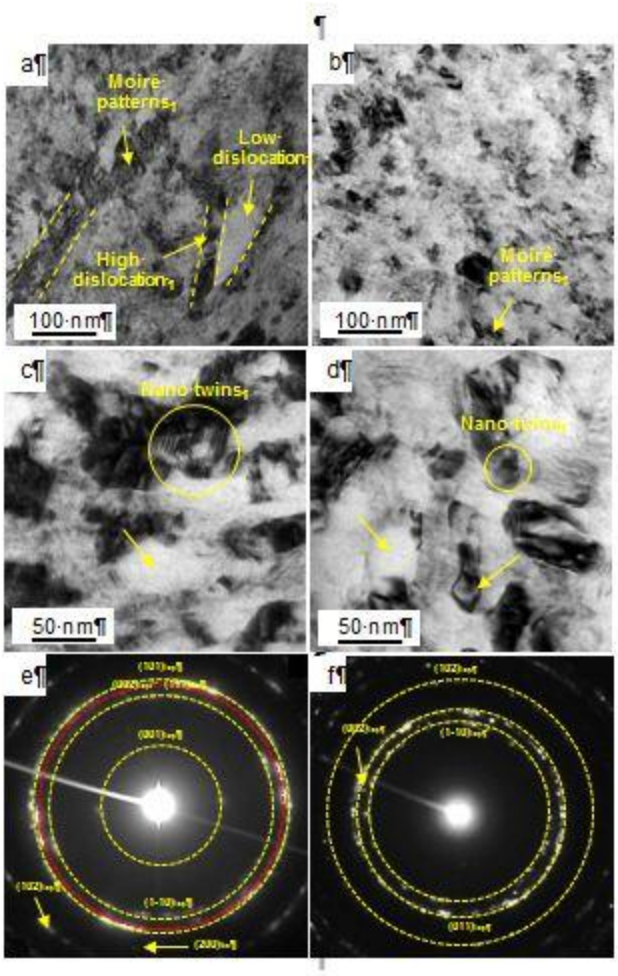

Fig. 6

Accepted manuscript